Simulation and experimental characterization of a dual-mode two-section amplified feedback laser with mode separation over 100 GHz

Biwei Pan (潘碧玮), Liqiang Yu (余力强), Dan Lu (陆 丹), Limeng Zhang (张莉萌),
and Lingjuan Zhao (赵玲娟)*

*Key Laboratory of Semiconductor Materials Science, Institute of Semiconductors,
Chinese Academy of Science, Beijing 100083, China*
Corresponding author: ljzhao@semi.ac.cn

A tunable two-section amplified feedback laser, which employs an amplifier section as the integrated feedback cavity, is designed and fabricated for dual-mode operation with mode separation of 100 GHz. Detailed simulations and experimental characterizations on the performance of the laser are presented. Promising dual-mode emission with continuous tuning range over 16 GHz (87.41–103.64 GHz) is experimentally demonstrated.

OCIS codes: 140.3490, 250.5960, 250.5300, 070.4560.
doi: 10.3788/COL201412.110605.

Mode-beating dual-wavelength semiconductor lasers, which can be used for optical microwave generation[1,2] and all-optical clock recovery[3–6], have attracted much attention in recent years. Many schemes based on monolithic two-section distributed feedback (TS-DFB) lasers[7,8], mode-locked semiconductor lasers (MLLs)[9,10], or amplified feedback lasers (AFLs)[11–13] have been reported for generating mode beating and achieving all-optical clock recovery. TS-DFBs, which can provide large frequency tuning ranging from dozens of gigahertzs to hundreds of gigahertzs, need relatively complicated fabrication process since two different grating periods or different ridge widths shall be introduced into the two DFB sections. TS-DFBs can hardly generate two modes with equal intensity at most working frequencies as the mode from rear-end DFB laser must pass through the front-end DFB laser. MLLs can generate high-quality optical pulse with ultrahigh frequency[14,15]. However, it has a very narrow frequency tuning range and the beating frequency is very sensitive to cavity length.

It is theoretically predicted by the Lang–Kobayashi model[16,17] that a DFB laser with a short feedback cavity can generate dual-mode output due to the coexistence of two external cavity modes having the same threshold gain. From this point of view, a three-section monolithic integrated AFL, which consists of a DFB section, a phase section, and an amplified feedback section[11], was designed and experimentally demonstrated. This kind of device can generate high-quality beating note with continuous frequency tuning range of 7–11.5 GHz[18], 17–34 GHz[12], and 12–45 GHz[11], respectively. However, three-section AFLs can hardly generate dual-mode with beating frequency above 100 GHz, due to the relatively long delay feedback time. To achieve higher beating frequency, shorter feedback cavity length with enough feedback strength is needed.

Here a tunable TS-AFL for mode beating around 100 GHz is designed and fabricated. Detailed simulations and experimental characterizations of the laser are presented. Stable dual-mode emission with beating frequency around 100 GHz can be generated in this device. Mode spacing of the laser can be tuned by the currents applied on the DFB section and the amplifier section. Good agreement between the simulation and experimental results has been demonstrated. It has been experimentally shown that a continuous tuning of beating frequency from 87.41 to 103.64 GHz can be realized via the control of currents injected into each laser section.

As shown in Fig. 1, the TS-AFL consists of a complex-coupled DFB laser section operating as a master laser and an amplifier section as the integrated feedback cavity.

To achieve high-frequency mode beating around 100 GHz, the length of feedback cavity should be carefully chosen. It has been shown that beating frequency (f) is determined by feedback strength (K) and delay feedback time (τ) according to the relations[11]

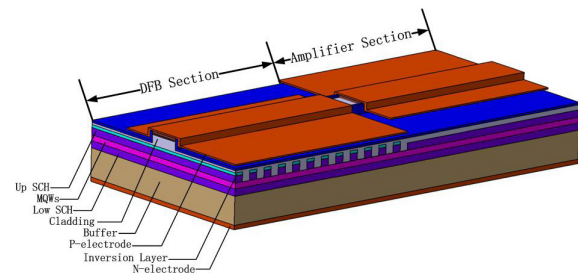$$K = K_0 \cdot \left| \frac{\pi \cdot f \cdot \tau}{\sin(\pi \cdot f \cdot \tau)} \right|, \tag{1}$$

Fig. 1. Schematic diagram of a TS-AFL.

$$K_0 = \frac{1}{2C_f} \cdot \frac{L_{\text{DFB}}}{L_{\text{EC}}}, \tag{2}$$

where K_0 represents the minimum feedback strength to achieve dual-mode lasing, which is determined by the effective lengths of DFB section (L_{DFB}), the effective lengths of external cavity (L_{EC}), and the feedback sensitivity C_f of DFB section. According to Eqs. (1) and (2), the external cavity length as a function of different feedback strengths (K/K_0) for $f = 100$ GHz is plotted in Fig. 2. The factor (K/K_0) is generally 2–3 for this kind of device[11–13]. Thus, we choose 240 and 220 μm as the length of amplifier and DFB sections, respectively, to achieve 100 GHz mode separation, with the consideration of the 20 μm long isolation region between two laser sections.

The time-domain traveling wave equations can be used to model multi-section DBR lasers[19] and AFLs[12]. Good agreement between simulations and experimental results has been reported. In our simulation, we used the commercial package VPI transmission Maker™ which was utilized to simulate the Q-switched self-pulsation characteristic of the AFL for clock recovery in Ref. [20]. In the transmission-line laser model (TLLM), the device is discretized in both time and space with a time step Δt and a spatial step $\Delta z = \nu \times \Delta t$, respectively, where ν is the velocity of signal propagation in the waveguide. The scattering nodes are obtained after such discretization. After that, traveling wave equation in each scattering node is solved, and then each scattering node is optically coupled together. The time step Δt is equal to the reciprocal of the sampling rate, which is an important parameter in the simulation. All the simulations are carried out using a sampling rate of 2560×10^9 Hz, corresponding to a node-length of 34.46 μm. The TLLM parameters used in DFB section and amplifier section are provided in Table 1. Among these parameters, active region width (the width of multiple quantum wells (MQWs) active region), DFB section length, and amplifier section length are set based on the manufacture data and device design mentioned above. Meanwhile, index and
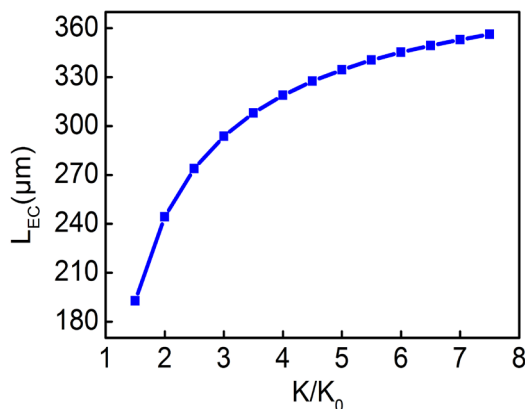
Table 1. Parameters of TLLM

Parameter	Value
Nominal Wavelength	1.55252 μm
DFB Section Length	220 μm
Amplified Section Length	240 μm
Active Region Width	3 μm
Confinement Factor of MQWs	0.07
Confinement Factor of SCH	0.56
Index Grating Coupling Coefficient	10,000 1/m
Gain Grating Coupling Coefficient	1000 1/m
Internal Loss	2500 1/m
Linewidth Enhancement Factor	4.5
Chirp Reference Carrier Density	2×10^{24} 1/m³
Linear Recombination Coefficient	3×10^8 1/s
Bimolecular Recombination Coefficient	1×10^{-16} m³/s
Auger Recombination Coefficient	1×10^{-41} m⁶/s
Transparency Carrier Density	1×10^{24} 1/m³
Linear Material Gain Coefficient	30×10^{-21} m²
Nonlinear Gain Coefficient	1×10^{-23} m³

gain grating coupling coefficients are set by referring to Ref. [12], and other parameters, such as confinement factor of MQWs (ratio of the MQWs active region volume to the optical mode volume), confinement factor of separated confinement heterojunction (SCH; ratio of the SCH region volume to the optical mode volume), are set as the recommended value which is typical for a DFB laser with MQWs active region in the software.

The laser can work in a dual-mode lasing state by choosing appropriate injection current in each section. Figures 3(a) and (b) show the simulated spectra of the laser in both optical and electrical domains, when the DFB and amplifier section are biased at 38 and 36 mA, respectively. Dual-mode operation with a beating frequency of 100 GHz can be observed. The tuning ranges of the beating frequency under different currents of amplifier section (I_A) and DFB section (I_{DFB}) are shown in Figs. 4(a) and (b). When the current of the DFB section is fixed, the beating frequencies gradually increase with the increase in amplifier section currents. At a certain amplifier section current, the beating frequencies decrease with the increase in DFB currents. A beating-frequency tuning range from 85 to 110 GHz can be achieved with the change of injection currents into each section.

After simulation, a monolithic integrated TS-AFL is experimentally fabricated. A schematic view of the device is shown in Fig. 1. The device consists of two separate sections: a 220 μm DFB section and a 240 μm

Fig. 2. External cavity length (L_{EC}) as a function of feedback strength (K/K_0) for 100 GHz mode beating.
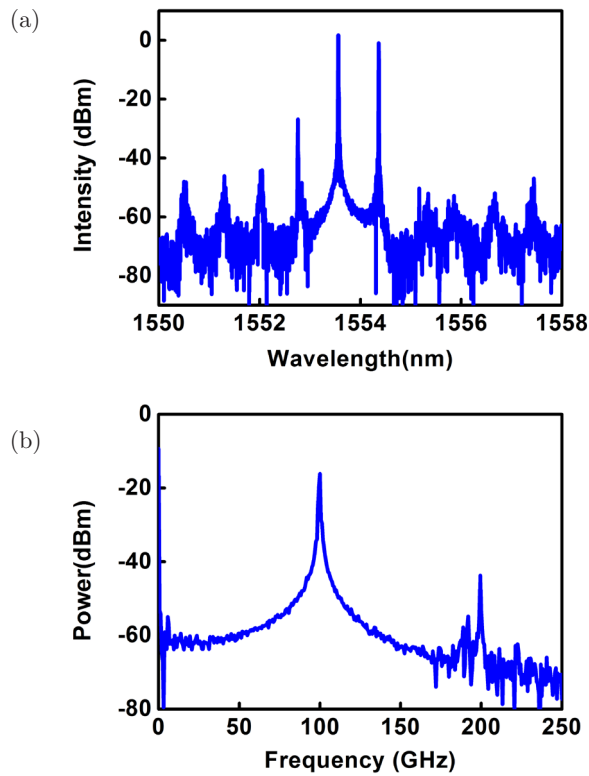
(a)

(b)

Fig. 3. Simulated spectra of the device in (a) optical and (b) electronic domains, with the injected currents in DFB and amplifier section at 38 and 36 mA, respectively.

(a)

(b)

Fig. 4. Tunability of the device under different current injections into the (a) amplifier section (I_{DFB} fixed at 38 mA) and (b) DFB section (I_A fixed at 16 mA).

amplifier section, which are separated by a 20 μm long isolation region.

The device material is grown on an S-doped n-type InP substrate by the metal-organic chemical vapor deposition (MOCVD). The epitaxial structure consists of five pairs of compressed strain InGaAsP MQWs sandwiched between two SCH layers. The complex-coupled DFB grating is made by holography on the upper SCH layer in DFB section. Then a p-type cladding InP layer and a heavy doping p-type InGaAs contact layer are re-grown by MOCVD. A 3 μm ridge waveguide is formed by wet etching. The electrical isolation between the two laser sections is realized by etching the p-type InGaAs contact layer off and He+ implantation. A Ti–Au metal layer is sputtered on the p-type InGaAs contact layer to form a p-contact electrode. Then the wafer is thinned and Au–Ge–Ni metal is evaporated on the backside. Finally, the n-contact electrode is formed after rapid temperature annealing. The wafer is cleaved to separate chips with no facet coating.

The device under test is mounted on a Cu heat sink with a thermoelectric cooler which maintains the working temperature at 25 °C. The output power and voltage of p–n junction as a function of DFB current (with floated amplifier section) are shown in Fig. 5. The threshold current of the device is about 51 mA. A sudden increase in optical power at 51 mA is due to saturated absorption of the amplifier section.
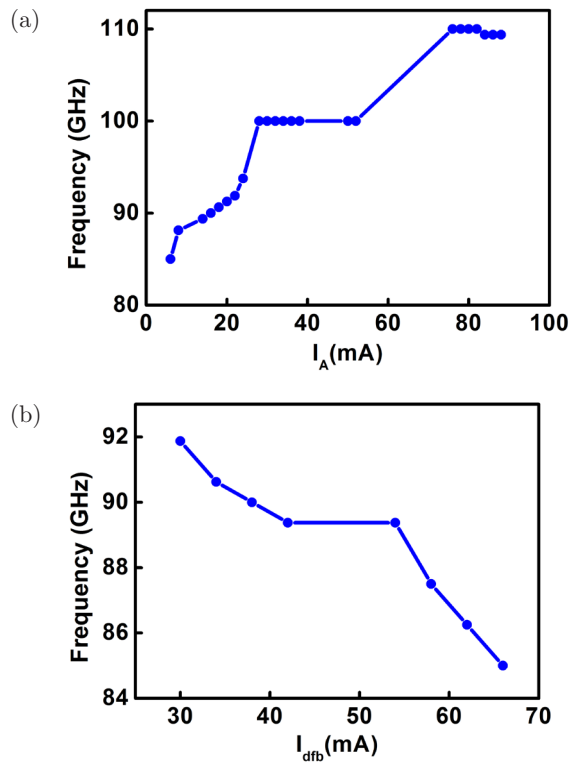
Optical output is coupled out through a tapered single-mode fiber from the DFB side and characterized with an optical spectrum analyzer (Advantest Q8384). When the currents applied in the DFB and amplifier section are 40 and 22 mA, respectively, the typical optical spectrum is as shown in Fig. 6. The wavelength difference ($\Delta\lambda$) between the two main modes is 0.8 nm, which corresponds to 100 GHz beating frequency.

Then the tunability of the mode spacing of the device is studied. As shown in Fig. 7(a), with the increase
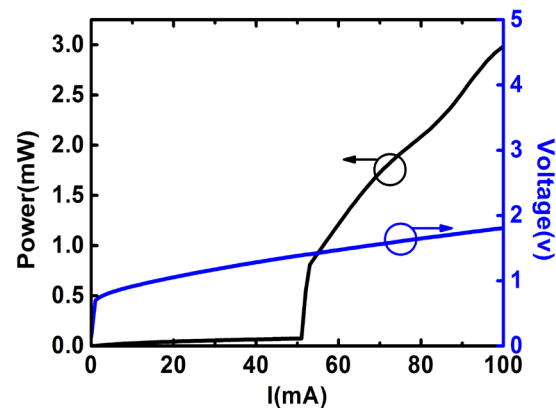

Fig. 5. Measured curve of light power output and voltage of p–n junction as a function of injection current of DFB section at unbiased amplifier section.
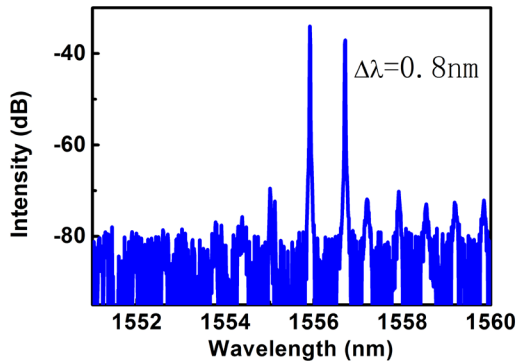
Fig. 6. Measured optical spectrum of the TS device, when $I_{\text{DFB}} = 40$ mA and $I_{\text{A}} = 22$ mA.

in amplifier section current of I_{A} at a fixed DFB current $I_{\text{DFB}} = 55$ mA, the long-wavelength mode (LM) sweeps continuously to the longer wavelength, whereas the other peak stays un-shifted. At the beginning of the dual-mode state ($I_{\text{A}} = 24$ mA), the power of LM is very small. With the increase in I_{A}, LM gradually becomes stronger, whereas the short-wavelength mode (SM) becomes relatively weaker. Finally, LM dominates the lasing mode and the laser switches to single-mode state. During the tuning process, the beating frequency increases from 87.41 to 98.65 GHz at dual-mode

state when I_{A} is tuned from 27 to 37 mA, as shown in Fig. 7(b). It can be concluded from the results that LM is the external cavity mode determined by I_{A}. Frequency tuning is realized by the red-shift of LM with the increasing I_{A} due to the increased feedback strength and thermal effect. The LM will be the dominant mode when I_{A} exceeds certain value and the gain of the LM is larger than the SM.

The optical spectra of the dual-mode laser with different I_{DFB} when $I_{\text{A}} = 30$ mA are shown in Fig. 8(a). The increase in I_{DFB} from 48 to 58 mA leads to a red-shift of the SM from 1556.08 to 1556.25 nm. The strength of SM becomes gradually stronger with the increasing I_{DFB}, while the LM gradually weakens. The SM finally dominates the lasing mode at $I_{\text{DFB}} = 58$ mA. The corresponding beating frequency of dual-mode state decreases from 98.65 to 89.90 GHz as shown in Fig. 8(b). As discussed above, with increased I_{DFB} at a fixed I_{A}, the power of SM becomes stronger resulting from the increasing mode gain, and the wavelength of SM red-shift results from the decreasing feedback strength as well as thermal effect. The SM would be dominant when I_{DFB} exceeds the value and the gain of SM is larger than LM.

As can be seen from Figs. 3, 4, 6, and 7, the experimental results agree well with the simulation predictions. Stable dual-mode emission with beating
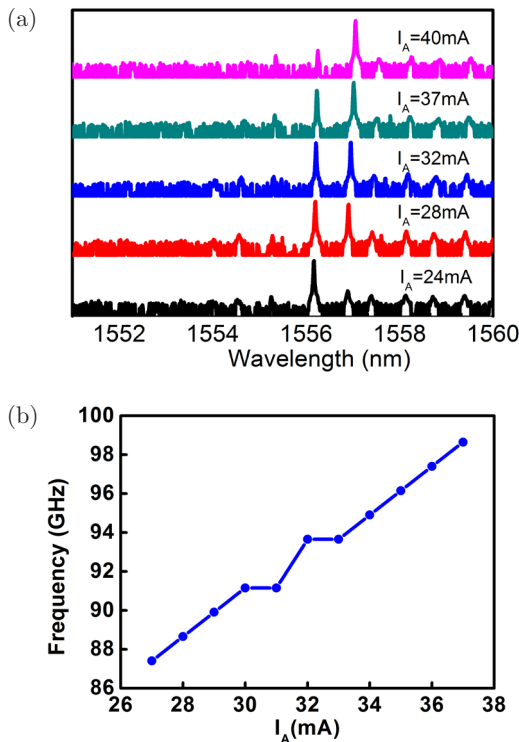

Fig. 7. (a) Output spectra of the device with different amplifier section currents, while DFB current is fixed at 55 mA and (b) corresponding tuning curve of the beating frequency at dual-mode state.
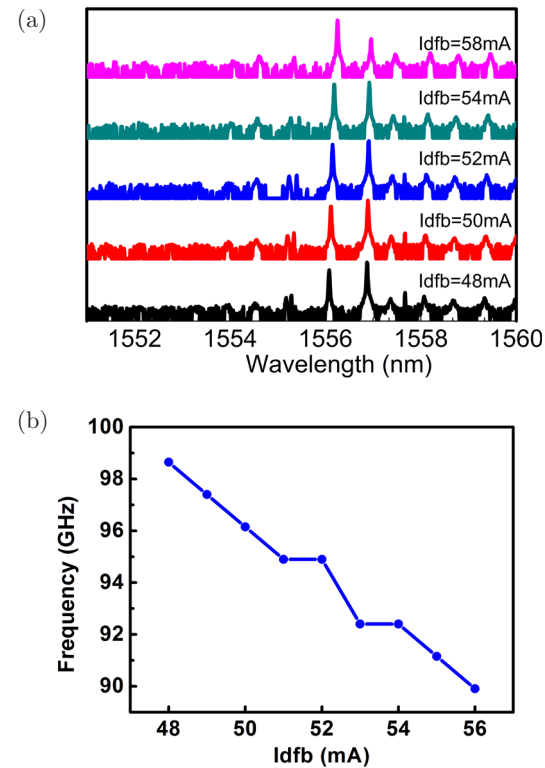

Fig. 8. (a) Output spectra of the device with different DFB section currents, while amplifier current is fixed at 30 mA and (b) corresponding tuning curve of the beating frequency at dual-mode state.
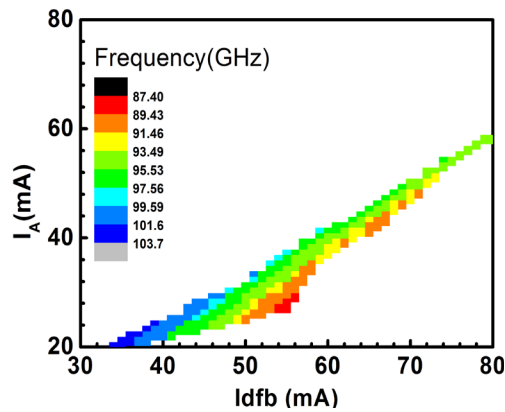
Fig. 9. Tuning map in the plane of I_{DFB} and I_A. Different levels of colors respond to beating frequencies of 87.4–103.7 GHz.

frequency around 100 GHz can be obtained in both simulations and experiments. The experimental tendencies of beating frequencies with different injection currents of each laser section are quite inconsistent with the simulation.

The contour of beating frequency with respect to I_{DFB} and I_A is shown in Fig. 9. A continuous beating frequency tuning from 87.41 to 103.64 GHz can be generated when I_{DFB} is tuned from 30 to 80 mA while I_A is tuned from 20 to 80 mA. The laser may work in single-mode, multi-mode, F-P modes, or chaos states in regions outside the contour area in Fig. 9. The strength difference between the two main modes corresponding to Fig. 9 is shown in Fig. 10. Dual-mode lasing states with the same mode power can be selected in the different beating frequencies.

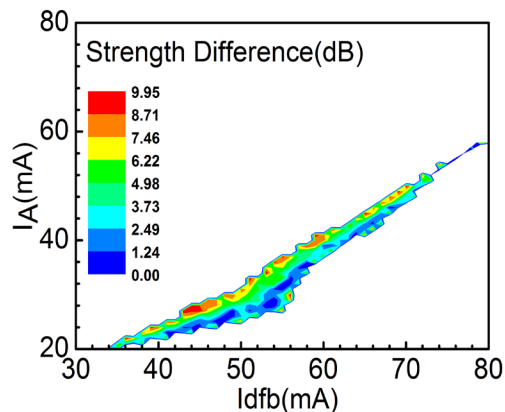In conclusion, a tunable TS-AFL with beating frequency around 100 GHz is designed and fabricated. Dual-mode lasing is obtained in both simulations and experiments. Mode-beating frequencies from 87.41 to 103.61 GHz are realized by changing the currents applied on DFB and amplifier sections. The TS-AFL can be found potential applications in the all-optical clock recovery and optical microwave generations.

References

1. G. Grosskopf, D. Rohde, R. Eggemann, S. Bauer, C. Bornholdt, M. Mohrle, and B. Sartorius, IEEE Photon. Technol. Lett. **12,** 1692 (2000).
2. D. S. Yee, Y. A. Leem, S. B. Kim, D. C. Kim, K. H. Park, S. T. Kim, and B. G. Kim, Opt. Lett. **29,** 2243 (2004).
3. W. M. Mao, Y. H. Li, M. Al-Mumin, and G. F. Li, J. Lightwave Technol. **20,** 1705 (2002).
4. L. Q. Yu, D. Lu, L. J. Zhao, Y. Li, C. Ji, J. Q. Pan, H. L. Zhu, and W. Wang, IEEE Photon. Technol. Lett. **25,** 576 (2013).
5. J. Qiu, C. Chen, L. Zhao, Y. Sun, D. Lu, C. Lou, and W. Wang, Appl. Opt. **51,** 2894 (2012).
6. L. Yu, Y. Li, J. Zang, D. Lu, B. Pan, and L. Zhao, Chin. Opt. Lett. **12,** 081402 (2014).
7. D. H. Kong, H. L. Zhu, S. Liang, H. G. Zhang, Y. Sun, H. Wang, W. Zhang, and L. J. Zhao, J. Phys. D: Appl. Phys. **42,** 125105 (2009).
8. B. Sartorius, M. Mohrle, and U. Feiste, IEEE J. Sel. Top. Quant. Electron. **1,** 535 (1995).
9. H. Tsuchida, IEEE Photon. Technol. Lett. **18,** 1687 (2006).
10. T. Wang, C. Lou, L. Huo, and Y. Gao, Chin. Opt. Lett. **2,** 69 (2004).
11. O. Brox, S. Bauer, M. Radziunas, M. Wolfrum, J. Sieber, J. Kreissl, B. Sartorius, and H. J. Wunsche, IEEE J. Quant. Electron. **39,** 1381 (2003).
12. D. S. Yee, Y. A. Leem, S. T. Kim, K. H. Park, and B. G. Kim, IEEE J. Quant. Electron. **43,** 1095 (2007).
13. C. Chen, Y. Sun, L. Zhao, J. Pan, J. Qiu, S. Liang, W. Wang, and C. Lou, Opt. Commun. **284,** 5613 (2011).
14. M. Peccianti, A. Pasquazi, Y. Park, B. E. Little, S. T. Chu, D. J. Moss, and R. Morandotti, Nat. Commun. **3,** 765 (2012).
15. Y. Ding, Y. Wang, Z. Li, L. Tan, J. Liu, and S. Li, Chin. Opt. Lett. **1,** 286 (2003).
16. R. Lang and K. Kobayashi, IEEE J. Quant. Electron. **16,** 347 (1980).
17. A. A. Tager and K. Petermann, IEEE J. Quant. Electron. **30,** 1553 (1994).
18. D. S. Yee, Y. A. Leem, S. B. Kim, E. Sim, H. G. Yun, D. C. Kim, and K. H. Park, IEEE Photon. Technol. Lett. **17,** 1151 (2005).
19. P. Bardella and I. Montrosset, IEEE J. Sel. Top. Quant. Electron. **11,** 361 (2005).
20. I. Monfils and J. C. Cartledge, J. Lightwave Technol. **27,** 619 (2009).

Fig. 10. Strength difference of two main modes in the plane of I_{DFB} and I_A. Different levels of colors respond to strength difference of two main modes from 0 to 10 dB.